

Conjugation Pathway of Benzobisoxazoles in Polymer Donors Mediates the Charge Management and Enables Organic Solar Cells with Record Certified Efficiency

Miao Liu, Lunbi Wu, Yulong Hai, Yongmin Luo, Yao Li, Rouren Chen, Yue Ma, Tao Jia,*
 Qingduan Li, Sha Liu, Ruijie Ma,* Yue-Peng Cai, Jiaying Wu, Gang Li,*
 and Shengjian Liu*

Charge management plays a pivotal role in achieving high-performance bulk heterojunction (BHJ) organic solar cells (OSCs). In this study, two efficient polymer donors are designed, P[4,8]BBO and P[2,6]BBO, by regulating the conjugation pathways of benzobisoxazoles (BBO) through 4,8- and 2,6-linkages, respectively. Comparing to P[2,6]BBO, the isomer of conjugation pathway has been proved to enable P[4,8]BBO a shallower highest occupied molecular orbital (HOMO) energy level of -5.20 eV, significantly enhanced luminescence efficiency, and reduced aggregation property. These improvements lead to a dramatic increase in device efficiencies from 2.6% for P[2,6]BBO:eC9-2Cl to 19.0% for P[4,8]BBO:eC9-2Cl. The combined characterizations show that a better comprehensive charge management can be reached in P[4,8]BBO:eC9-2Cl-based OSCs, yielding a significantly higher short-circuit current density (I_{SC}) and fill factor (FF) parameters compared to P[2,6]BBO:eC9-2Cl-based ones. Furthermore, P[4,8]BBO demonstrates good applicability and can achieve an impressive efficiency of 19.4% in all-polymer solar cells with a third-party certified efficiency of 19.1%. This work highlights the critical role of conjugation pathway isomerism in mediating polymeric properties and advancing the development of high-performance multifunctional photovoltaic materials.

1. Introduction

As a new power generation technology, organic solar cells (OSCs) hold significant promise in photovoltaic market. This potential stems from advantages, including flexibility, lightweight, color adjustability, and compatibility with roll-to-roll printing technologies.^[1–7] Thanks to the innovation of non-fullerene acceptors with strong light absorption in near-infrared range (NIR, 700–1000 nm), high electron mobility, tunable energy level, and reduced non-radiative energy loss, OSCs have reached power conversion efficiencies (PCEs) of up to 20%.^[8–14] Considering the strong light absorption of state-of-the-art Y-series acceptors in the near-infrared region, developing efficient wide bandgap (WBG) polymer donors that exhibit good light absorption complementarity with Y-series acceptors is of importance.^[15–18] The alternating copolymerization of “weak acceptors” and

M. Liu, R. Chen, Y. Ma, T. Jia, Q. Li, Y.-P. Cai, S. Liu
 School of Chemistry
 Guangzhou Key Laboratory of Materials for Energy Conversion and Storage
 Key Laboratory of Electronic Chemicals for Integrated Circuit Packaging
 South China Normal University (SCNU)
 Guangzhou 510006, P. R. China
 E-mail: shengjian.liu@m.scnu.edu.cn

L. Wu, T. Jia
 School of Optoelectronic Engineering
 School of Mechanical Engineering
 Guangdong Polytechnic Normal University
 Guangzhou 510665, P. R. China
 E-mail: tjia@gpnu.edu.cn

Y. Hai, Y. Luo, Y. Li, J. Wu
 Advanced Materials Thrust
 Function Hub
 The Hong Kong University of Science and Technology (Guangzhou)
 Nansha, Guangzhou 511400, P. R. China

S. Liu
 Dongguan Key Laboratory of Interdisciplinary Science for Advanced Materials and Large-Scale Scientific Facilities
 School of Physical Sciences
 Great Bay University
 Dongguan, Guangdong 523000, P. R. China

R. Ma, G. Li
 Department of Electrical and Electronic Engineering
 Research Institute for Smart Energy (RISE)
 Photonic Research Institute (PRI)
 The Hong Kong Polytechnic University
 Hong Kong, P. R. China
 E-mail: ruijie.ma@polyu.edu.hk;gang.w.li@polyu.edu.hk

 The ORCID identification number(s) for the author(s) of this article can be found under <https://doi.org/10.1002/adma.202503702>

© 2025 The Author(s). Advanced Materials published by Wiley-VCH GmbH. This is an open access article under the terms of the Creative Commons Attribution License, which permits use, distribution and reproduction in any medium, provided the original work is properly cited.

DOI: [10.1002/adma.202503702](https://doi.org/10.1002/adma.202503702)

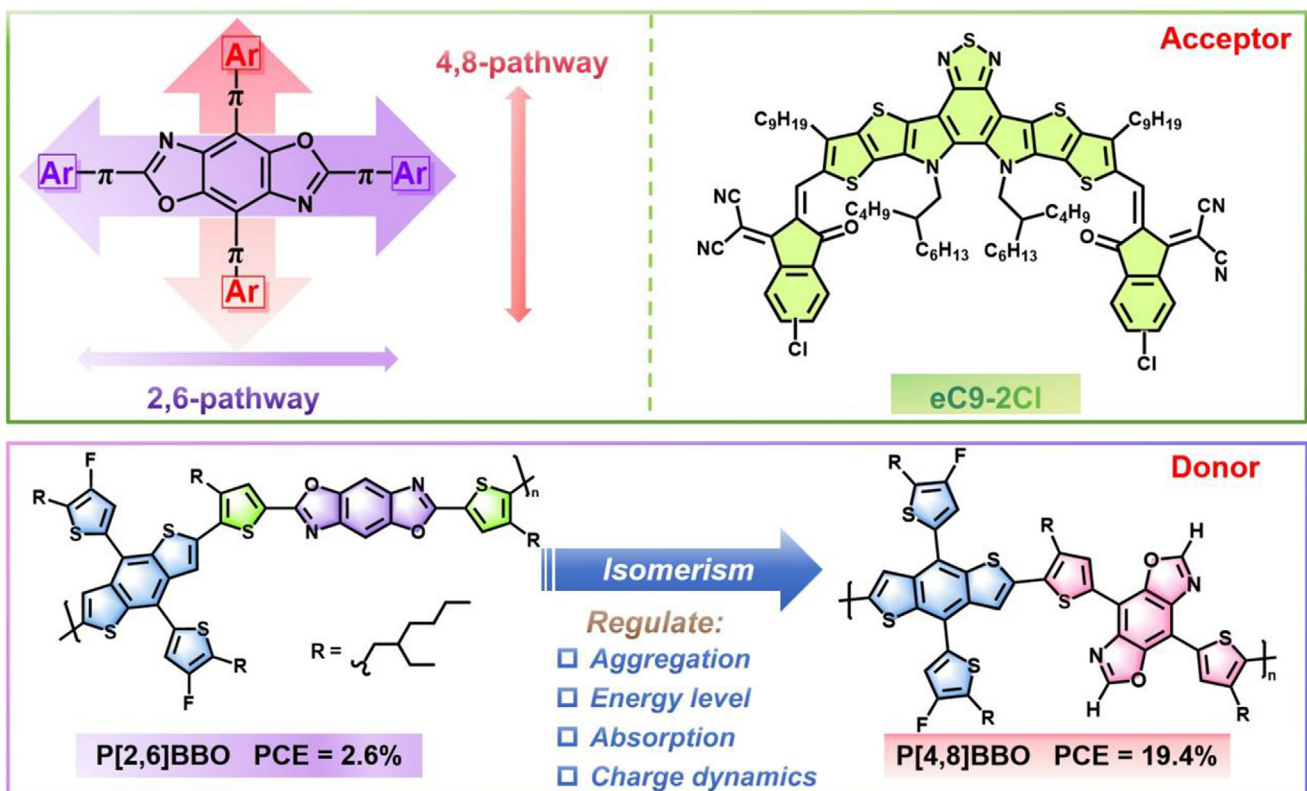


Figure 1. The two conjugation pathways of benzobisoxazole (BBO) and the chemical structures of eC9-2Cl and polymeric isomers P[2,6]BBO and P[4,8]BBO.

“weak donors” is one of the most effective strategies for tailoring the optical band gap and absorption spectra, and reaching efficient polymer donors (PM6,^[19] D18,^[20] PTQ10,^[21] PBTz-F,^[22] and their derivatives).

Isomerism is a common phenomenon in organic and polymeric molecules and can be used to effectively tailor physicochemical properties of target materials.^[23–27] For example, Zhan et al. reported two acceptors, FNIC1 and FNIC2, with thiophene positional isomerism on the fused-ring cores, demonstrating that optimizing the thiophene arrangement improves the absorption spectrum, electron mobility, affinity, and π – π stacking, leading to a higher power conversion efficiency (PCE).^[28] He et al. reported an electron-accepting unit, TTDO, an isomer of building block for PM6 polymer, and the derived polymer donor named PBTT-F can endow a red-shifted absorption spectrum, more ordered packing compared to PM6.^[29] Recently, we demonstrated that the isomerism from 2,1,3-benzothiadiazole to 1,2,3-benzothiadiazole and naphtho [1,2-c:5,6-c']bis([1,2,5]thiadiazole) to naphtho [1,2-c:5,6-c']bis([1,2,3]thiadiazole) motifs can endow significantly distinctions of molecular configuration, energy level structure, luminescent efficiency, and aggregation characteristic of target polymers and lead to complete difference in device performance.^[30,31] Among various isomerism phenomena, conjugation pathway isomerism is a crucial yet underexplored aspect. In fact, the conjugation pathway influences the effective conjugation length, electron delocalization, dipole moment, and steric hindrance, thereby significantly impacting absorption spectra, molecular en-

ergy levels, aggregation behavior, and luminescence properties. For example, poly(N-alkyl-carbazole) with 2,7-linkages exhibits a red-shifted absorption spectrum, a narrower optical band gap, and a shallower highest occupied molecular orbital (HOMO) energy level compared to its 3,6-linked isomer.^[32,33] Benzobisazole (BBO) is known as a coplanar electron-deficient aromatic heterocycle, featuring a central benzene ring fused with two oxazole rings.^[34–36] As shown in Figure 1, the BBO structure typically exhibits 2,6- and 4,8-conjugation pathways. However, most documented BBO-based polymer donors have been π -extended through the 2,6-conjugation pathway, which generally leads to relatively poor photovoltaic performance.^[37,38] In contrast, the transition from 2,6-conjugation to 4,8-conjugation may result in (i) increased steric hindrance due to the perpendicular orientation of the BBO building block and (ii) a shallower HOMO energy level caused by the exclusion of the BBO unit from the conjugated backbone. These merits potentially help to tailor energy levels, aggregation features, and also the BHJ morphology.

In this contribution, we focus on the isomerism of the conjugation pathway in benzobisoxazole (BBO) building blocks and report two novel polymers, P[2,6]BBO and P[4,8]BBO (Figure 1), which are π -extended through 2,6- and 4,8-conjugation pathways, respectively. The effect of this conjugation pathway distinction on the polymers’ photoelectric properties and photovoltaic performance is systematically investigated. The transition from 2,6-conjugation to 4,8-conjugation enables precise energy level control, ensuring a sufficient driving force for exciton

dissociation and balanced aggregation for an optimized blend film morphology, collectively contributing to superior charge management. Consequently, the P[4,8]BBO-based OSCs achieved a significantly enhanced efficiency of 19.0%, with a short-circuit current density (J_{SC}) of 28.1 mA cm^{-2} and a fill factor (FF) of 77.5%, outperforming their P[2,6]BBO-based counterparts. Moreover, the polymer donor P[4,8]BBO also demonstrated excellent performance in all-polymer solar cells, achieving a high efficiency of 19.4%, with a third-party verified efficiency of 19.1%. Our work demonstrates that benzobisoxazole (BBO) is a promising building block for designing efficient polymer donors, and that regulating conjugation pathways can effectively turn decay into magic in tailoring polymeric photoelectric properties.

2. Results and Discussion

2.1. Molecular Design, Synthesis and Characterization

To investigate the geometrical conformations and electronic structures, density functional theory (DFT) calculations were performed on two models,^[2,6]BBO-FBDT and^[4,8]BBO-FBDT, which represent the repeat units of P[2,6]BBO and P[4,8]BBO, respectively. First, the optimal conformations (Figure 2a) reveal that both models exhibit small torsion dihedral angles ($\theta_1: 0.05^\circ\text{--}0.27^\circ$ and $\theta_2: 0.82^\circ\text{--}0.51^\circ$) and nearly coplanar structures. The single-crystal structure analyses further confirm the related model compounds demonstrate coplanar geometrical conformations with twist angles ranging from 3° to 6° between BBO unit and thiophene. Moreover, the^[4,8]BBO-based model compound forms H-aggregates with shorter $\pi\text{-}\pi$ stacking distances of 3.507 \AA and stronger intermolecular hydrogen bonding, which enhances charge transport between molecules (see Figure S30, Supporting Information). As shown in Figure 2b,^[4,8]BBO-FBDT demonstrates a lower potential energy surface (PES) compared to^[2,6]BBO-FBDT, indicating that the geometrical configuration of^[4,8]BBO-FBDT is controllable. This suggests that the aggregation states of P[4,8]BBO can potentially be regulated by simply adjusting the solution processing parameters during device fabrication.^[39] Second, as shown in Figure 2c,^[4,8]BBO-FBDT possesses a shallower HOMO energy level of -5.29 eV which provides a larger driving force for hole transfer from the acceptor to the donor. Third,^[4,8]BBO-FBDT demonstrates a larger dipole moment (μ) of 1.72 Debye compared to^[2,6]BBO-FBDT (0.23 Debye), facilitating intermolecular stacking and efficient charge transport.^[40\text{--}43] Fourth, Figure 2e shows the hole and electron density distributions, indicating that both^[2,6]BBO-FBDT and^[4,8]BBO-FBDT exhibit a larger hole-electron overlap (Sr-index) value of $0.71\text{--}0.74$. The transition dipole moments (TDMx) of^[2,6]BBO-FBDT are directed from the acceptor BBO to the donor benzodithiophene (FBDT), while the opposite direction significantly inhibits the electron redistribution within the donor FBDT. In contrast,^[4,8]BBO-FBDT shows large TDMx of 5.01 Debye , oriented from the donor FBDT to the acceptor BBO, which enhances the oscillator strength (f) to 1.58 and the light absorption coefficient to $0.655 \times 10^5 \text{ M}^{-1}\cdot\text{cm}^{-1}$ (see Figure 2d; Tables S1 and S2 and Figure S2, Supporting Information). Lastly, the intermolecular interactions between the donor and acceptor were analyzed using the Interaction Region Indicator (IRI). As illus-

trated in Figure 2f,g, the red part represents the repulsion caused by the steric effect between donors and acceptors. The van der Waals interactions of the donor/acceptor molecules mainly originates from the $\pi\text{-}\pi$ interactions of conjugated molecules.^[44] As predicted by the Independent Gradient Model based on Hirshfeld (IGMH),^[45] the^[4,8]BBO-FBDT/eC9-2Cl pair shows extremely strong $\pi\text{-}\pi$ interactions and strong delocalized features of π -electrons between the donor^[4,8]BBO-FBDT and acceptor eC9-2Cl molecules. While the interactions between^[2,6]BBO-FBDT and eC9-2Cl are relatively weaker. The parameter $\delta G_{\pi\cdots\pi}$ was introduced to describe the contribution of the $\pi\text{-}\pi$ interaction. The^[4,8]BBO-FBDT/eC9-2Cl pair has a significantly larger $\delta G_{\pi\cdots\pi}$ value of 32.47% than that of^[2,6]BBO-FBDT/eC9-2Cl pair with $\delta G_{\pi\cdots\pi}$ of only 25.52% . The higher $\delta G_{\pi\cdots\pi}$ implies the^[4,8]BBO-FBDT/eC9-2Cl pair has better $\pi\text{-}\pi$ stacking and stronger intermolecular interactions, which enhanced the charge transfer, separation, and generation between donor and acceptor.

Based on computational analysis, the conjugation pathway isomerism can precisely modulate the photoelectric properties. Scheme 1 outlines the synthetic routes for the key intermediate 4,8-dibromobenzo[1,2-d:4,5-d']bis(oxazole) (4), the target polymer P[4,8]BBO, and the control polymer P[2,6]BBO. Briefly, the key intermediate (4) is synthesized from 2,3,5,6-tetrabromocyclohexa-2,5-diene-1,4-dione 1) through an amine and bromine-exchange reaction with ammonium hydroxide (NH_4OH), followed by quinone reduction using sodium dithionite ($\text{Na}_2\text{S}_2\text{O}_4$), and dehydrative condensation with triethyl orthoformate. Notably, these three reaction steps achieve a high overall yield of 77%, and all the key intermediates can be purified through recrystallization without the need for column chromatography, significantly reducing both material and labor costs for the synthesis. Afterwards, compound (4) undergoes a Stille coupling reaction with tributyl(4-(2-ethylhexyl)thiophen-2-yl)stannane (5) to yield intermediate (6), which is then brominated to produce the key monomer M1. The control monomer M2 can be synthesized through a three-step process, as previously reported.^[38] M1 and M2 were then polymerized via Stille coupling with the monomer BDTF-DSn to produce P[4,8]BBO and P[2,6]BBO, respectively. The chemical structures have been well confirmed through ^1H NMR, ^{13}C NMR, high-resolution mass spectrometry (HRMS), and high temperature gel permeation chromatography (GPC) characterizations (see Figures S3 and S4 and S10–S29 and Table S3, Supporting Information). P[4,8]BBO and P[2,6]BBO exhibit excellent solubility in common organic solvents, including chlorobenzene, chloroform, toluene, and o-xylene, enabling their solution processability for the fabrication of OSCs.

2.2. Optical and Electronic Properties

Figure 3a,b illustrates the UV-vis absorption spectra of the P[2,6]BBO and P[4,8]BBO donors and acceptor eC9-2Cl, which exhibit complementary absorption across 400–1000 nm, enabling efficient light absorption in bulk heterojunction (BHJ) photoactive layers. Compared to P[2,6]BBO, P[4,8]BBO exhibits a bathochromic shift of $\approx 40 \text{ nm}$ in both solution and films, accompanied by a reduction in the optical band gap (E_g^{opt}) from 2.10 to 1.95 eV (see Table 1). Although both polymer donors exhibit

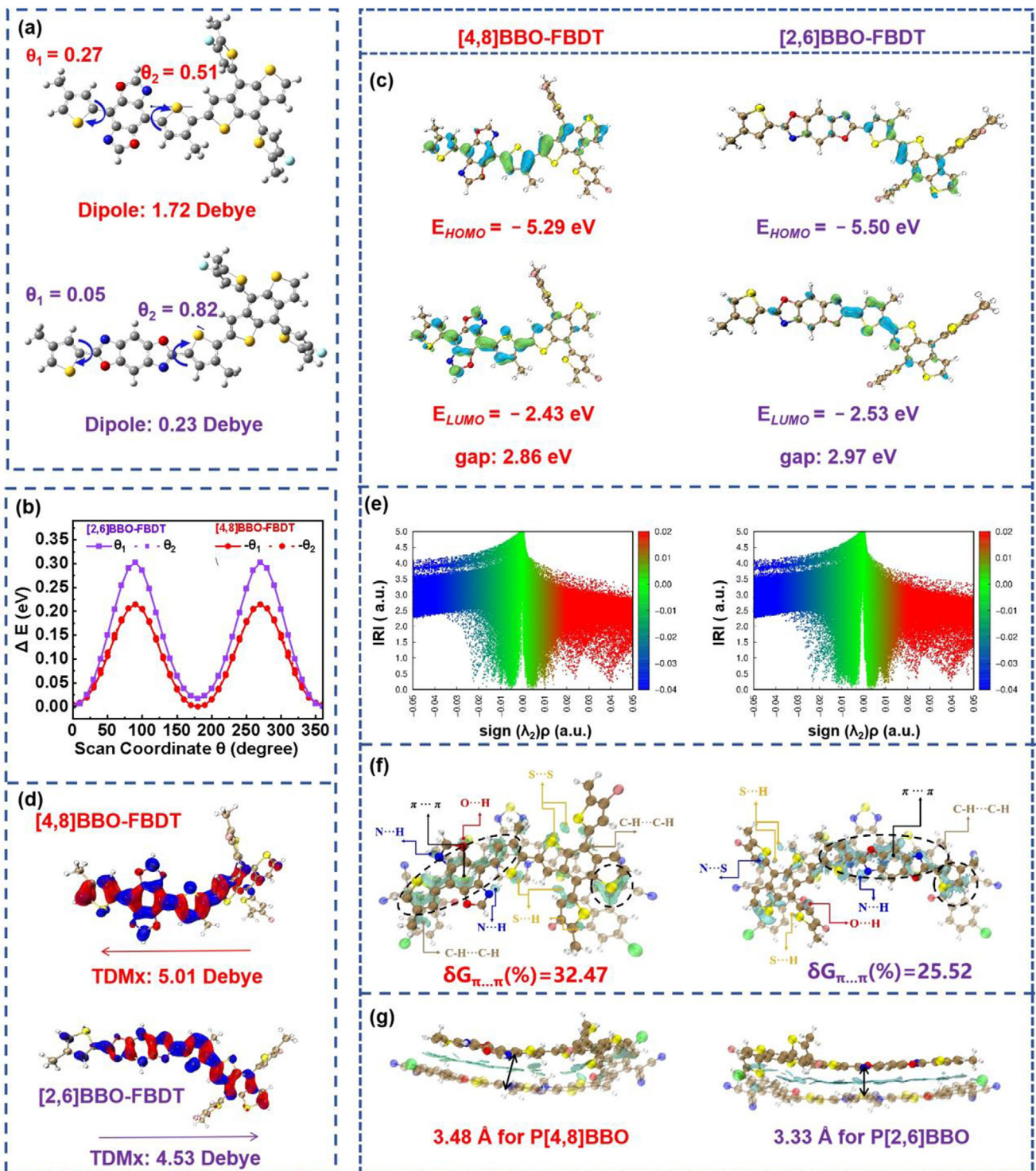
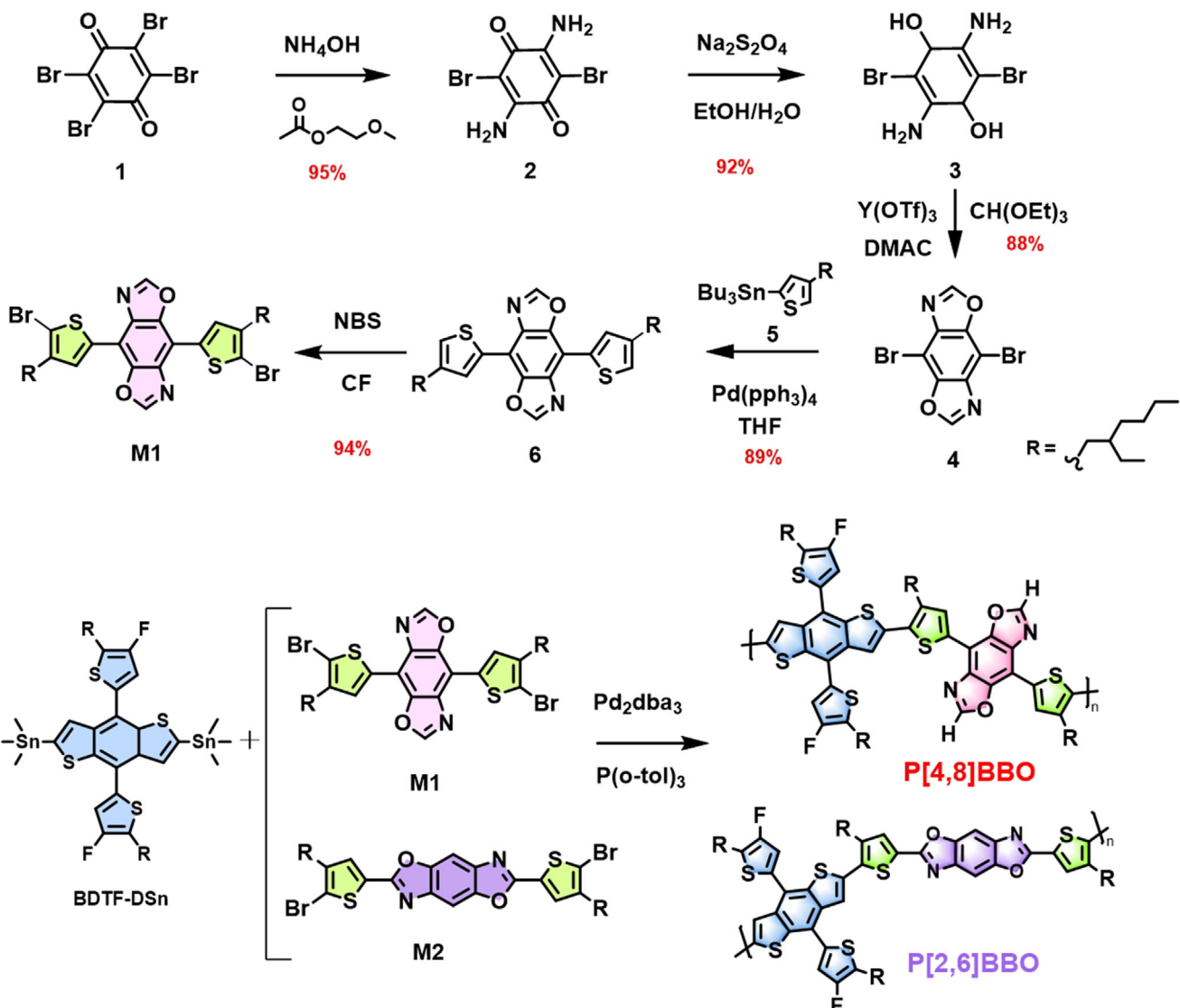


Figure 2. a) The optimal geometrical conformations and predicted dipole moment (μ), b) the potential energy surface (PES) scans of the torsion dihedral angles θ_1 and θ_2 , c) the frontier molecular orbitals and energy level values, d) the hole and electron density distributions of $S_0 \rightarrow S_1$ transition and transition dipole moments (TDMx) in x axis of backbone direction (blue and red represent the electron and hole distributions), e) Independent Gradient Model based on Hirshfeld (IGMH) and f) IRI isosurface map colored by sign (λ_2) ρ of dimer made with donor and acceptor, g) the schematic diagram of molecular interactions between donors and acceptors.



Scheme 1. Synthetic routes for the key intermediate **M1** and the two isomeric polymers, **P[4,8]BBO** and **P[2,6]BBO**.

0–1 and 0–0 peaks, corresponding to the ICT effect and $\pi-\pi^*$ transition, their aggregation behaviors differ. **P[4, 8]BBO** shows lower I_{0-0}/I_{0-1} ratios in both solution and film, compared to **P[2, 6]BBO**, thereby indicating that **P[4, 8]BBO** forms controllable aggregates. Figure 3c,d presents the temperature-dependent absorption spectra in solution. The I_{0-0}/I_{0-1} ratio of **P[2, 6]BBO** remains high at 114.2% even at 100 °C, while that of **P[4, 8]BBO** significantly decreases from 106.7% at 25 °C to 71.9% at 100 °C (see Table S4, Supporting Information), confirming that the aggregation behavior is effectively modulated, potentially contributing to improved blend film morphology.^[46] The ionization potential (IP) values and energy level alignments, measured by photoelectron spectroscopy (PESA), are shown in Figure 3e,f. The control polymer donor **P[2, 6]BBO** exhibits a higher IP of 5.42 eV, corresponding to a deeper HOMO level and the energy offset for hole transfer between acceptor **eC9-2Cl** and **P[2, 6]BBO** is only 0.26 eV, below the 0.3 eV typically required

for efficient charge separation.^[47,48] In contrast, **P[4, 8]BBO** exhibits a smaller IP of 5.20 eV, corresponding to a shallower HOMO level, which increases the HOMO energy offset between acceptor **eC9-2Cl** and **P[4, 8]BBO** to 0.48 eV, potentially providing a stronger driving force for efficient hole transfer and charge generation.

Charge transfer between the donor and acceptor was further investigated through photoluminescence (PL) quenching experiments. As shown in Figure 3g,h, the high PL quenching efficiencies of **P[2,6]BBO** (~96.15%) and **P[4,8]BBO** (~98.30%) in the presence of **eC9-2Cl** indicate efficient electron transfer from the donor domains to the acceptor domains. For hole transfer, the PL quenching efficiencies of **eC9-2Cl** with **P[2,6]BBO** and **P[4,8]BBO** are 35.87% and 96.13%, respectively. The significantly higher quenching efficiency in the **P[4,8]BBO:eC9-2Cl** system suggests more efficient hole transfer from **eC9-2Cl** to **P[4,8]BBO**, consistent with the larger HOMO energy offset between **P[4,8]BBO** and

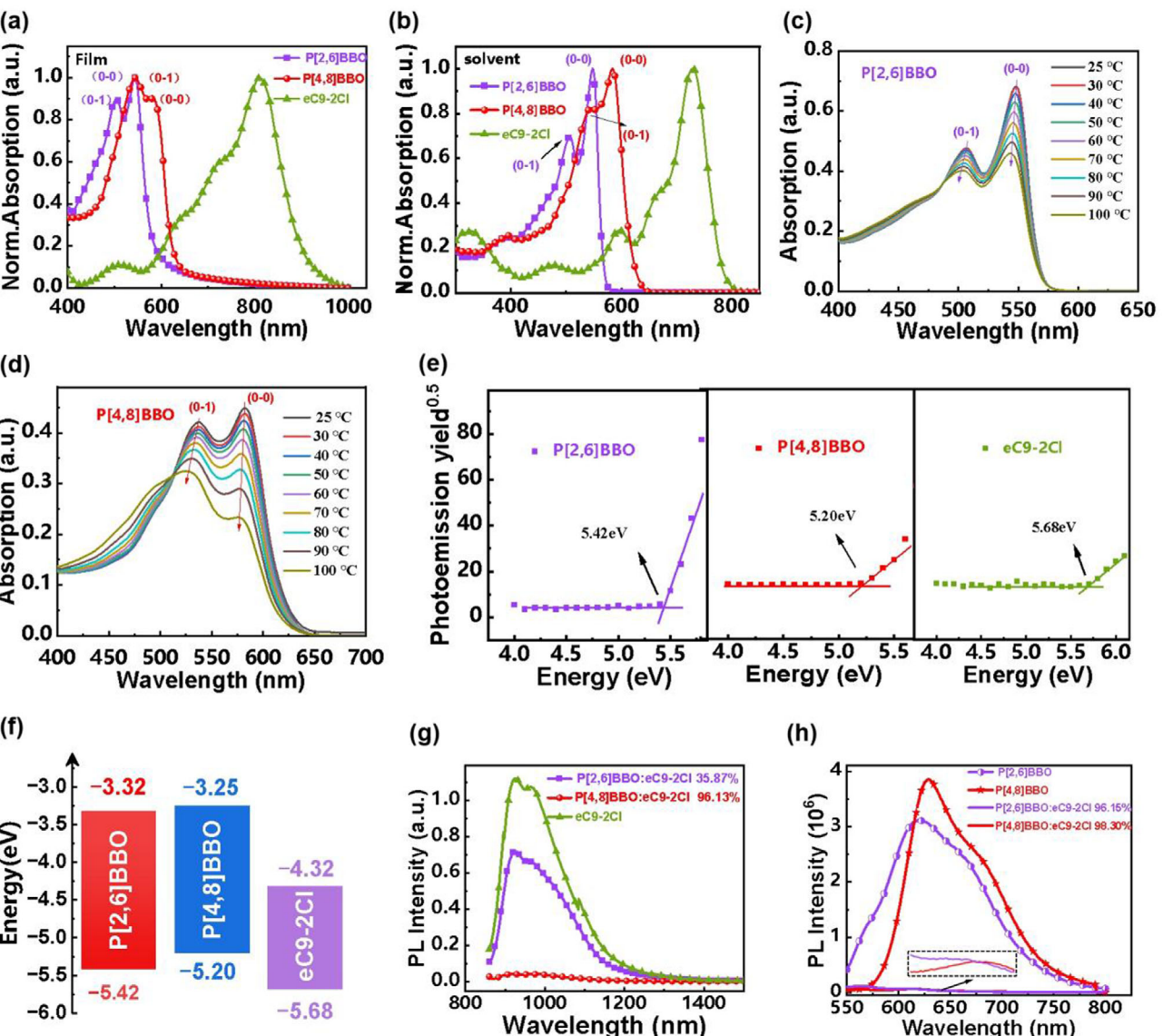


Figure 3. a,b) The UV–vis absorption spectra of P[4,8]BBO, P[2,6]BBO, and eC9-2Cl in solid films and solutions; c,d) the temperature-dependent UV–vis absorption spectra of P[4,8]BBO and P[2,6]BBO in solution; e,f) the PESA curves and energy levels for P[4,8]BBO, P[2,6]BBO, and eC9-2Cl; the photoluminescence (PL) quenching of g) acceptor eC9-2Cl in the presence of donors and h) donors in the presence of acceptor eC9-2Cl as in optimized BHJ thin films.

eC9-2Cl. These results highlight the critical role of the polymer donor's conjugation pathway in regulating energy levels and optimizing charge management.^[49]

2.3. Photovoltaic Performance

To investigate the impact of conjugation pathways on photovoltaic performance, P[4,8]BBO and P[2,6]BBO were employed as donors in OSCs (Figure 4a), with eC9-2Cl as the acceptor. The significantly different current density versus voltage (J – V) curves in Figure 4b demonstrate the profound influence of conjugation pathways on device performance. As summarized in Table 2, P[2,6]BBO achieved a higher open-circuit voltage (V_{OC})

of 0.95 V due to its deeper HOMO level (-5.42 eV), but it exhibited a low short-circuit current density (J_{SC}) of 5.0 mA cm^{-2} and a poor fill factor (FF) of 55.2%, resulting in a very low power conversion efficiency (PCE) of 2.6%. Notably, previous studies have shown that BBO-based polymer donors with a 2,6-conjugation pathway typically achieve modest efficiencies $\approx 3\%$ (Table S5, Supporting Information), which has limited the appeal of benzobisazole (BBO) as a candidate for designing high-performance polymer donors.^[37,50,51] As shown in Table 2 and Figure 4b, the P[4,8]BBO-based device achieved a slightly lower V_{OC} of 0.87 V but exhibited significant improvements in J_{SC} and FF parameters. Specifically, the J_{SC} increased from 5.0 to 28.1 mA cm^{-2} , and the FF improved from 55.2% to 77.5%, resulting in a remarkable PCE of 19.0%—approximately seven times higher than that of

Table 1. The molecular weight, optical and electronic properties of P[2,6]BBO, P[4,8]BBO, and eC9-2Cl.

Polymer	M_n [kDa]	M_w [kDa]	λ_{max}^{sol} [nm]	λ_{max}^{film} [nm]	λ_{onset}^{film} [nm]	E_g^{opt} ^{a)} [eV]	IP ^{b)} [eV]
P[2,6]BBO	37.3	65.9	548	504/544	590	2.10	5.42
P[4,8]BBO	59.0	108.3	584	544/582	636	1.95	5.20
eC9-2Cl	—	—	729	811	911	1.36	5.68

a) $E_g^{opt} = 1240/\lambda_{onset}^{film}$; b) IP determined by PESA.

the P[2,6]BBO-based device. Notably, this PCE value represents the highest efficiency reported for OSCs using BBO-based polymer donors to date (Table S5, Supporting Information). These results demonstrate that benzobisazole (BBO) can be a promising building block for designing efficient polymer donors by inge-

nious structural design. The external quantum efficiency (EQE) spectra (Figure 4c) were measured to validate the J_{SC} values. The P[2,6]BBO device shows a weak EQE response, with values below 10% across the 400–950 nm range, consistent with its low photoluminescence (PL) quenching efficiency and inefficient

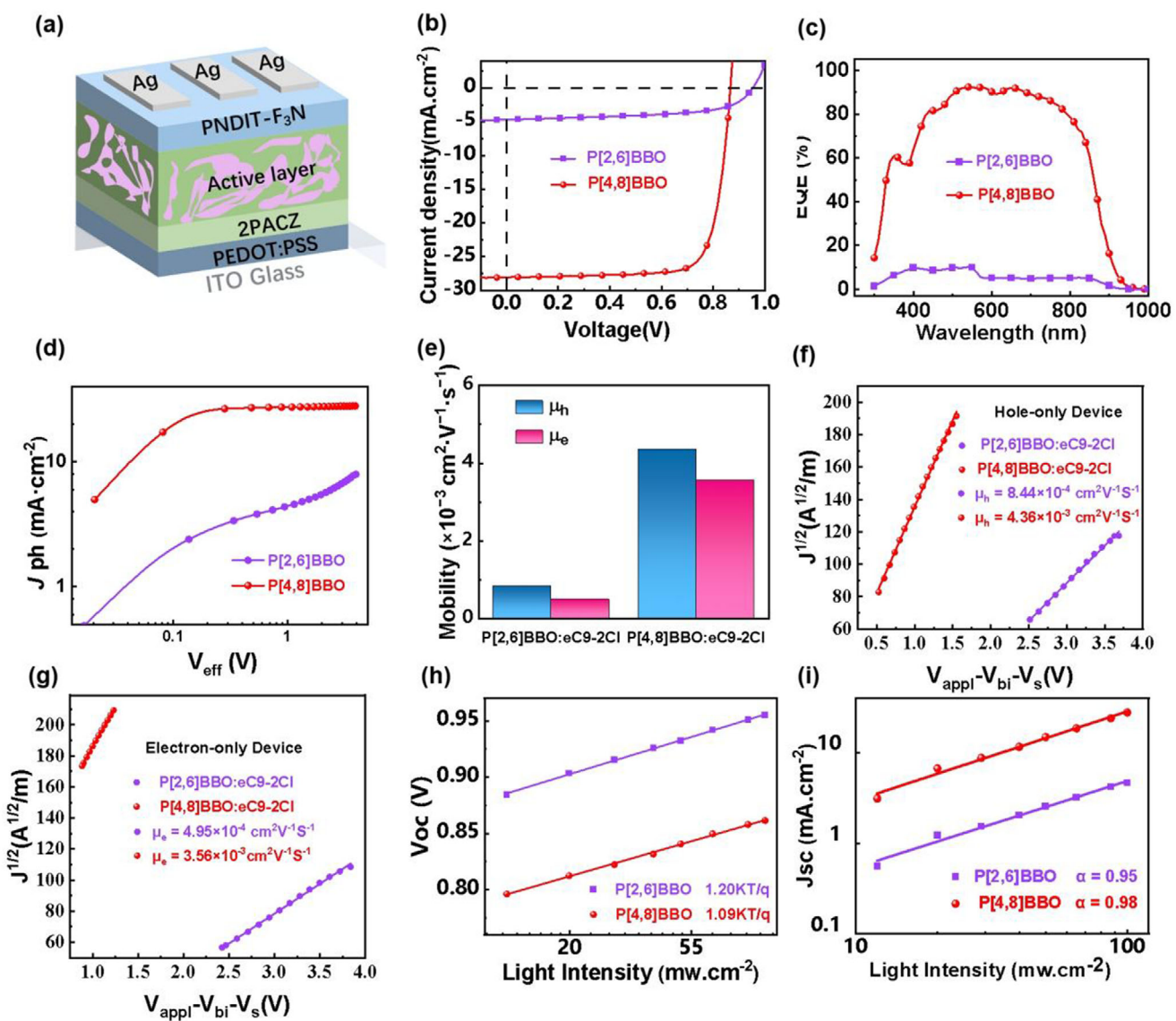


Figure 4. a) The device structure of binary OSCs, the b) J – V curves, c) EQE spectra, d) J_{ph} vs. V_{eff} curves, e) hole and electron mobilities, f,g) dark current density versus voltage curves that were fitted by SCLC model, h,i) dependence of V_{OC} and J_{SC} as a function of incident light intensities (P_{light}) for the P[2,6]BBO- and P[4,8]BBO-based devices.

Table 2. The photovoltaic parameters of P[2,6]BBO- and P[4,8]BBO-based binary OSCs.

Donor	V_{OC} [V]	J_{SC} [mA cm^{-2}]	FF [%]	PCE [%]	J_{SC}^{EQE} [mA cm^{-2}]
P[2,6]BBO	0.95	5.0	55.2	2.6 (2.4 ± 0.3) ^{a)}	2.5
P[4,8]BBO	0.87	28.1	77.5	19.0 (18.9 ± 0.1) ^{a)}	27.2

^{a)} the average values based on 16 independent devices.

charge separation. In contrast, the P[4,8]BBO device achieves a significantly enhanced EQE response, exceeding 80% over the 500–800 nm range, indicating highly efficient photocurrent generation. The integrated photocurrents of 2.5 mA cm^{-2} for P[2,6]BBO and 27.2 mA cm^{-2} for P[4,8]BBO further confirm the superior performance of the P[4,8]BBO-based device.

2.4. Charge Generation, Transportation, and Recombination

Charge generation and collection were analyzed to understand the differences in FF, J_{SC} , and efficiency. Figure 4d shows the photocurrent density (J_{ph}) as a function of effective voltage (V_{eff}). In the P[2,6]BBO device, J_{ph} increases slowly with V_{eff} and fails to saturate even at high V_{eff} , indicating inefficient charge generation

under built-in electric field.^[52] In contrast, the P[4,8]BBO device shows a rapid increase in J_{ph} with V_{eff} ($V_{eff} < 0.2 \text{ V}$) and saturates when $V_{eff} > 0.2 \text{ V}$, with J_{ph} becoming independent of V_{eff} , suggesting efficient charge collection at the electrodes. The charge generation probabilities ($P(E, T) = J_{ph}/J_{sat}$) are 98.2% for P[4,8]BBO and 62.5% for P[2,6]BBO. The higher $P(E, T)$ of P[4,8]BBO indicates more efficient charge generation and exciton dissociation, aligning with findings from ultrafast transient absorption studies (discussed later). Additionally, hole (μ_h) and electron (μ_e) mobilities were measured using space-charge-limited current (SCLC) method (Figure 4e–g). The P[4,8]BBO device exhibits μ_h and μ_e values of 4.36×10^{-3} and $3.56 \times 10^{-3} \text{ cm}^2 \cdot \text{V}^{-1} \cdot \text{s}^{-1}$, respectively, approximately five and seven times higher than those for the P[2,6]BBO devices. The μ_h/μ_e ratio is 1.21 for P[2,6]BBO and 1.22 for P[4,8]BBO, indicating more balanced charge transport in the

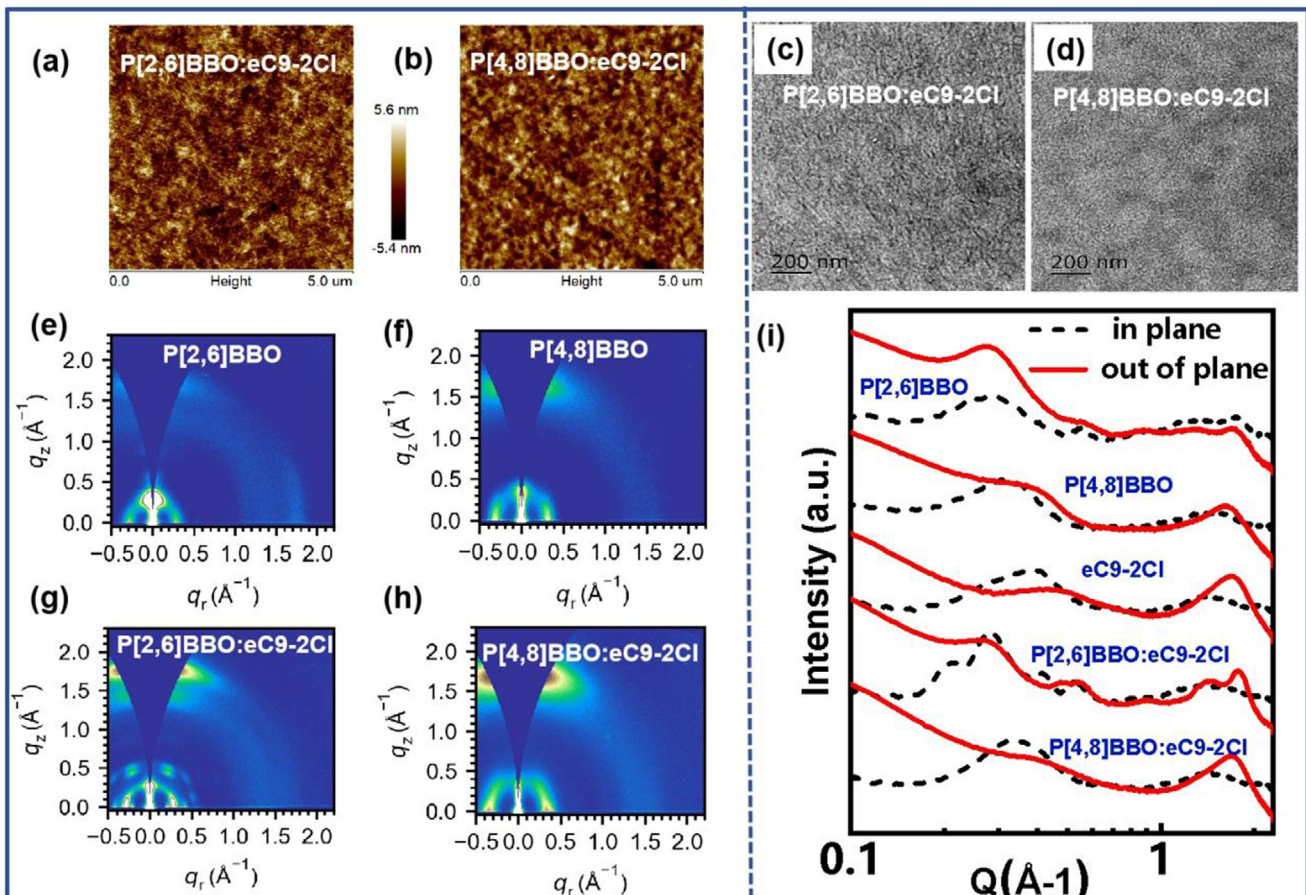


Figure 5. a,b) The AFM images and c,d) TEM images for the P[2,6]BBO:eC9-2Cl and P[4,8]BBO:eC9-2Cl BHJ films; the 2D-GIWAXS patterns: e) P[2,6]BBO, f) P[4,8]BBO, g) P[2,6]BBO:eC9-2Cl, and h) P[4,8]BBO:eC9-2Cl; i) 1D-GIWAXS line-cut profiles of neat and BHJ films.

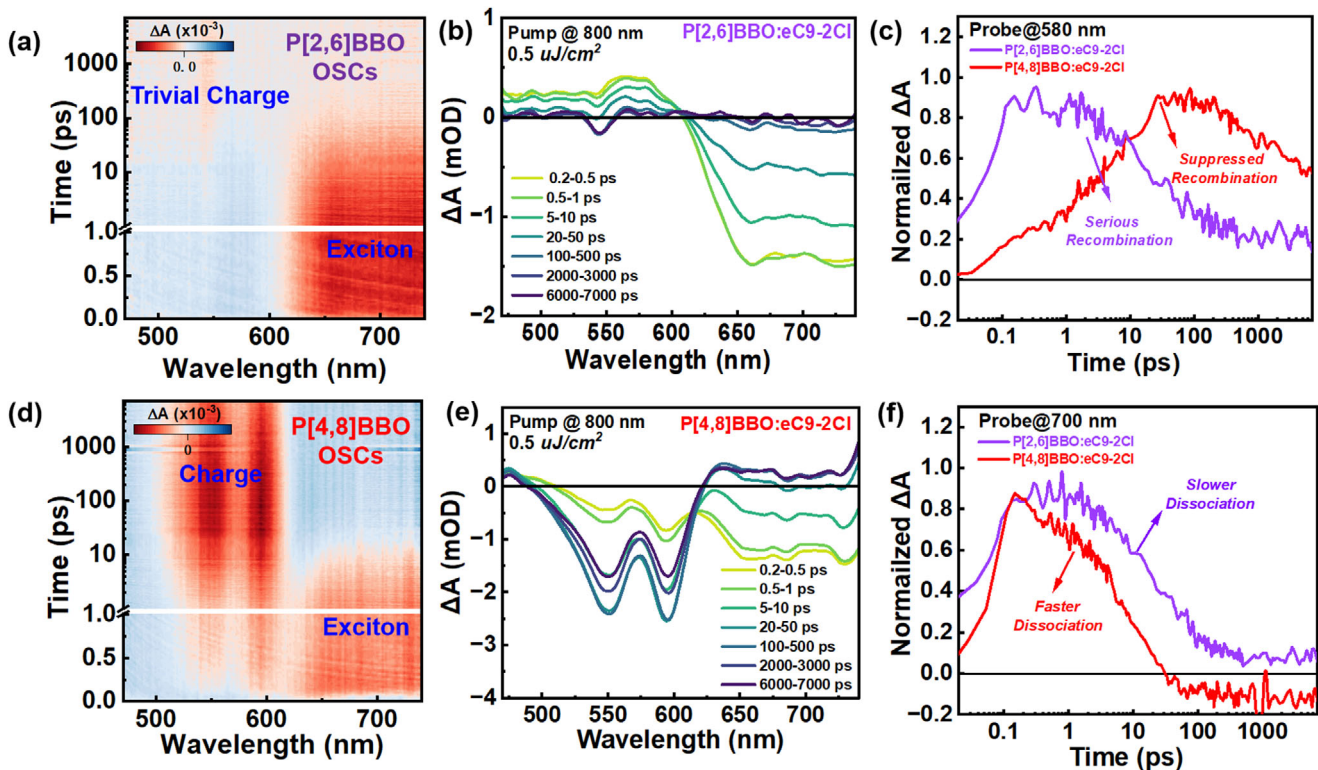


Figure 6. The femtosecond-resolved a-d) TA signals, b-e) TA spectra, c-f) TA dynamic curves probed at 580 and 700 nm of P[2,6]BBO:eC9-2Cl and P[4,8]BBO:eC9-2Cl BHJ films excited at 800 nm.

P[4,8]BBO devices. Furthermore, V_{OC} and J_{SC} were measured under varying light intensities (P_{light}). As shown in Figure 4h,i, the n value for the P[2,6]BBO device is 1.20, while for the P[4,8]BBO device, it is 1.09—closer to 1—indicating significantly reduced monomolecular and trap-assisted recombination.^[53] The α values are 0.95 for P[2,6]BBO and 0.98 for P[4,8]BBO, demonstrating suppressed bimolecular recombination in the P[4,8]BBO device.^[54] These results highlight that regulating the conjugation pathway finely tunes charge behavior, leading to improved FF and higher J_{SC} .

2.5. Morphological Characterization

Atomic force microscopy (AFM), transmission electron microscopy (TEM), and grazing incidence wide-angle X-ray scattering (GIWAXS) were used to analyze the BHJ morphologies. As shown in Figure 5a,b, the P[2,6]BBO- and P[4,8]BBO-based BHJ films exhibit similar root-mean-square (RMS) roughness values of 1.20 nm and 1.42 nm, respectively. Figure 5c,d shows no significant differences in TEM images. Figure 5e-i presents the 2D GIWAXS patterns, out-of-plane (OOP) and in-plane (IP) line-cut profiles, with key diffraction parameters summarized in Tables S7-S10 (Supporting Information). Both P[2,6]BBO and P[4,8]BBO neat films display distinct (100) lamellar stacking peaks ($q_x = 0.281\text{--}0.315 \text{ \AA}^{-1}$) in the IP direction and (010) $\pi\text{-}\pi$ stacking peaks ($q_z = 1.597\text{--}1.674 \text{ \AA}^{-1}$) in the OOP direction. P[2,6]BBO exhibits larger lamellar and $\pi\text{-}\pi$ stacking crystal coherence lengths (CCLs) of 51.53 and 33.07 Å, respectively,

while P[4,8]BBO shows a significantly reduced $\pi\text{-}\pi$ stacking CCL of 17.95 Å. In blend films, both P[2,6]BBO:eC9-2Cl and P[4,8]BBO:eC9-2Cl display clear (100) lamellar stacking peaks ($q_x = 0.282\text{--}0.344 \text{ \AA}^{-1}$) in the IP direction and (010) $\pi\text{-}\pi$ stacking peaks ($q_z = 1.673\text{--}1.769 \text{ \AA}^{-1}$) in the OOP direction, indicating strong face-on orientation that facilitates efficient vertical charge transport.^[55,56]

2.6. Exciton and Charge Carrier Dynamics

To investigate charge behavior, exciton and polaron dynamics were analyzed using ultrafast transient absorption spectroscopy (TAS). Donor and acceptor neat films were excited with 550 nm and 800 nm lasers, and their TA spectra (Figure S8, Supporting Information) showed characteristic ground-state bleach (GSB) peaks at 700 nm (eC9-2Cl), 550 nm (P[2,6]BBO), and 550 nm (P[4,8]BBO), which were used to track exciton and polaron dynamics.^[57,58] For P[2,6]BBO BHJ blends, an 800 nm laser excited the acceptor to generate eC9-2Cl excitons and induce hole transfer. As shown in Figure 6a,b,c,f: (i) the slow decay of the 700 nm peak in P[2,6]BBO:eC9-2Cl indicates prolonged eC9-2Cl exciton lifetime, (ii) the short-lived signal at 580 nm, with lifetime below 100 ps, suggests a pure exciton signal and inefficient polaron generation, which aligns with their spectral characteristics of eC9-2Cl, and (iii) the significant decay of the 580 nm peak indicates severe charge recombination. These factors correspond to the lower J_{SC} and FF found in P[2,6]BBO:eC9-2Cl OSCs. Turning to the investigation of P[4,8]BBO:eC9-2Cl BHJ film (Figure 6c-f):

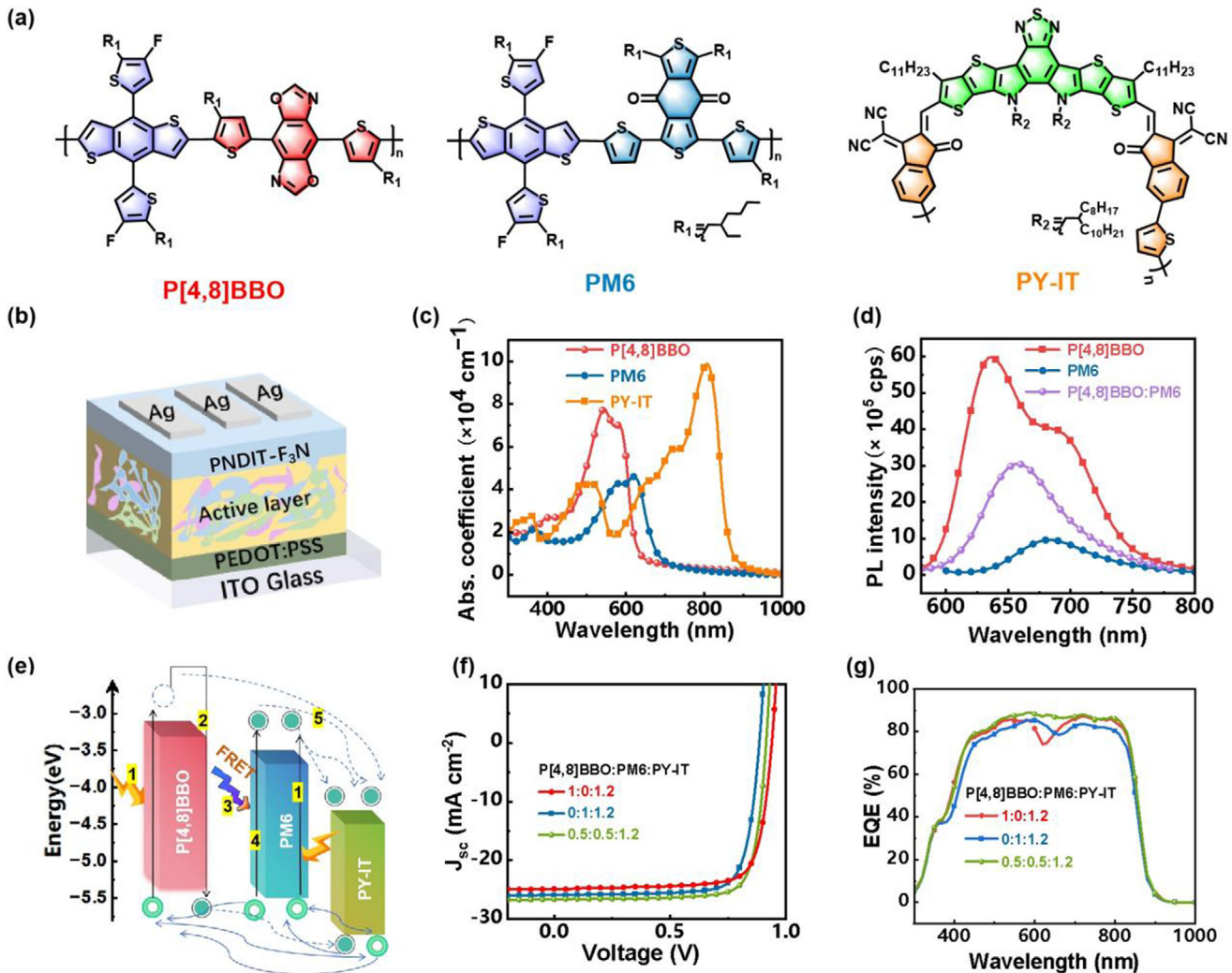


Figure 7. a) The chemical structure of P[4,8]BBO, PM6, PY-IT, b) the device structure of all-PSCs, c) UV–vis absorption spectra, d) photoluminescence (PL) spectra, e) energy level diagrams and possible pathways for Förster resonance energy transfer (FRET) and charge transfer, f) J–V curves and g) EQE spectra of binary and ternary cells based on P[4,8]BBO:PM6:PY-IT system.

(i) the rapid decay of the 700 nm peak indicates efficient eC9-2Cl exciton dissociation; (ii) the existence of long-lived signal at 580 nm, peaking within 20–50 ps, confirms efficient P[4,8]BBO polaron generation due to a sufficient driving force of 0.48 eV; (iii) the long-lived 580 nm signal suggests significantly suppressed recombination. These TAS results further highlight the critical role of the conjugation pathway in optimizing exciton dissociation, charge generation, and recombination, leading to enhanced J_{SC} and FF.

2.7. All-Polymer Solar Cells Characterizations

All-polymer solar cells (all-PSCs), featuring polymer donors and acceptors in the active layer, provide intrinsic long-term stability and flexibility.^[59–61] Given its excellent performance, P[4,8]BBO is further examined and utilized as the donor in all-polymer solar cells. As shown in Figure 7: (i) P[4,8]BBO exhibits a large

bandgap of 1.95 eV and strong absorption in the 450–620 nm range, complementing the absorption of the polymer donor PM6 (1.79 eV) and polymer acceptor PY-IT (1.42 eV); (ii) it shows strong fluorescence emission with a high photoluminescence quantum yield (PLQY) of 8%, significantly surpassing the PM6 (~2%); (iii) its photoluminescence in the 550–750 nm range well overlaps with the absorption spectra of PM6 (500–650 nm) and PY-IT (650–850 nm), facilitating Förster resonance energy transfer (FRET) from P[4,8]BBO excitons to PM6 (Figure 7c);^[62,63] (iv) its shallow energy level provides a larger driving force between P[4,8]BBO and PY-IT, potentially enhancing exciton dissociation while suppressing geminate recombination at the donor/acceptor interface. These advantages make P[4,8]BBO a promising donor for efficient binary and ternary all-PSCs.

Herein, P[4,8]BBO:PY-IT and PM6:PY-IT binary all-PSCs were fabricated to evaluate the potential of P[4,8]BBO. As shown in Figure 7f and summarized in Table 3, the benchmark

Table 3. Device performances of the optimal binary and ternary OSCs.

P[4,8]BBO:PM6:PY-IT	V_{OC} [V]	J_{SC} [mA cm^{-2}]	J_{SC}^{EQE} [mA cm^{-2}]	FF [%]	PCE [%]
1:0:1.2	0.89	25.9	25.1	78.2	17.9
0.5:0.5:1.2	0.91	26.6	25.9	79.7	19.4
0:1:1.2	0.94	24.9	24.2	77.9	18.2
Certified ^{a)}	0.89	27.0	—	79.5	19.1

^{a)} The ternary all-PSCs certificated by independent organizations.

PM6:PY-IT device achieved a high V_{OC} of 0.94 V, FF of 77.9%, and J_{SC} of 24.9 mA cm^{-2} , yielding a PCE of 18.2%. In comparison, P[4,8]BBO:PY-IT exhibited a V_{OC} of 0.89 V, FF of 78.2%, and J_{SC} of 25.9 mA cm^{-2} , resulting in a PCE of 17.9%, which is comparable to PM6-based devices. As shown in Figure 7g, the P[4,8]BBO:PY-IT blend achieves an EQE response over 80% across 450–900 nm but drops below 80% in the 600–660 nm range, whereas PM6:PY-IT shows a higher EQE above 85% in that range. To address these inefficiencies, a ternary all-PSC was fabricated by blending P[4,8]BBO and PM6 as donor components with PY-IT as the acceptor. This strategy enhances energy level pairing and broadens the EQE response. With an optimal weight ratio of 0.5:0.5:1.2 for P[4,8]BBO:PM6:PY-IT, the device efficiency improves from ≈18% in binary all-PSCs to 19.4% in ternary all-PSCs, driven by an increased FF of 79.7%, along with enhanced J_{SC} (26.6 mA cm^{-2}) and V_{OC} (0.91 V). The increased J_{SC} is directly confirmed by the EQE spectra in Figure 7g, where the ternary all-PSCs show enhanced EQE across the entire spectrum mainly due to synergistic charge generation at the P[4,8]BBO/PY-IT and PM6/PY-IT interfaces. Notably, a third-party certification verified an efficiency of 19.1% (Table 3, Figure S9, Supporting Information). To highlight its significance, Table S6 (Supporting Information) compares recent high-PCE all-PSCs certified by independent organizations. These findings further validate P[4,8]BBO as a promising polymer donor and demonstrate that tuning conjugation pathways is a powerful strategy for developing high-performance polymers.

3. Conclusion

In summary, by tuning the conjugation pathway isomerism of benzobisoxazoles (BBO), we designed two polymer donors, P[2,6]BBO and P[4,8]BBO. We demonstrated that conjugation pathway isomerism effectively regulates multiple properties of the target polymers: (1) it optimizes the energy levels, providing a larger driving force for efficient charge transfer and exciton dissociation; (2) it regulates the backbone conformation to ensure appropriate aggregation and BHJ morphology; and (3) it enhances luminous efficiency, enabling efficient Förster resonance energy transfer (FRET). As the fruit of these merits, P[4,8]BBO-based devices enable better charge management, with the derived binary OSCs achieving a high efficiency of 19.0%, significantly outperforming P[2,6]BBO-based devices (2.6%). Furthermore, P[4,8]BBO performs well in binary all-PSCs (≈18.0%) and improves ternary all-PSCs to 19.4%, with a third-party certified efficiency of 19.1%, ranking among the highest reported for all-PSCs. This study underscores the potential of conjugation pathway engineering as an effective strategy for optimizing polymer

properties, offering benefits not only for organic solar cells but also for broader organic electronic applications.

Supporting Information

Supporting Information is available from the Wiley Online Library or from the author.

Acknowledgements

S.L. acknowledges the financial support from the Natural Science Foundation of China (No. 21805097), the Guangdong Natural Science Foundation (No. 2021B1515120073), and the Guangdong Provincial Science and Technology Foundation (No. 2022A0505050068). T.J. acknowledges the financial support from the Natural Science Foundation of China (No. 21805099). R.M. gratefully acknowledges the support from the PolyU Distinguished Postdoctoral Fellowship (1-YW4C). J.W. thanks the Guangdong government and the Guangzhou government for funding (2021QN02C110), the Guangzhou Municipal Science and Technology Project (nos. 2023A03J0097 and 2023A03J0003).

Conflict of Interest

The authors declare no conflict of interest.

Author Contributions

M.L., L.W., and Y.H. contributed equally to this work. S.L., T.J., R.M., and G.L. proposed the research and designed the experiments. M.L. and T.J. synthesized the polymers. L.W., R.C., and R.M. fabricated the BHJ OSCs. Y.H. conducted the simulated calculation. Y.L. and Y.L. carried out the experiments of GISAXS and TAS measurements and analyzed the TAS data. Y.M. and Q.L. help to analyze the data. S.L., Y.-P. C., and G.L. provided the experiment condition. All authors commented on the manuscript.

Data Availability Statement

The data that support the findings of this study are available from the corresponding author upon reasonable request.

Keywords

charge management, conjugation pathway isomerism, organic solar cell, polymer donor

Received: February 24, 2025

Revised: May 2, 2025

Published online: June 4, 2025

- [1] C. Yan, S. Barlow, Z. Wang, H. Yan, A. K. Y. Jen, S. R. Marder, X. Zhan, *Nat. Rev. Mater.* **2018**, *3*, 18003.
- [2] L. Meng, Y. Zhang, X. Wan, C. Li, X. Zhang, Y. Wang, X. Ke, Z. Xiao, L. Ding, R. Xia, H.-L. Yip, Y. Cao, Y. Chen, *Science* **2018**, *361*, 1094.
- [3] Y. Liang, D. Zhang, Z. Wu, T. Jia, L. Lüer, H. Tang, L. Hong, J. Zhang, K. Zhang, C. J. Brabec, N. Li, F. Huang, *Nat. Energy* **2022**, *7*, 1180.
- [4] C. Liu, L. Shao, S. Chen, Z. Hu, H. Cai, F. Huang, *Prog. Polym. Sci.* **2023**, *143*, 101711.
- [5] J. Yi, G. Zhang, H. Yu, H. Yan, *Nat. Rev. Mater.* **2024**, *9*, 46.
- [6] B. Ma, Y. Yan, M. Wu, S. Li, M. Ru, Z. Xu, W. Zhao, *Adv. Funct. Mater.* **2025**, *35*, 2413814.
- [7] Z. Wang, D. Zhang, L. Yang, O. Allam, Y. Gao, Y. Su, M. Xu, S. Mo, Q. Wu, Z. Wang, J. Liu, J. He, R. Li, X. Jia, Z. Li, L. Yang, M. D. Weber, Y. Yu, X. Zhang, T. J. Marks, N. Stingelin, J. Kacher, S. S. Jang, A. Facchetti, M. Shao, *Science* **2025**, *387*, 381.
- [8] Y. Lin, J. Wang, Z. Zhang, H. Bai, Y. Li, D. Zhu, X. Zhan, *Adv. Mater.* **2015**, *27*, 1170.
- [9] Z. Xiao, X. Jia, D. Li, S. Wang, X. Geng, F. Liu, J. Chen, S. Yang, T. P. Russell, L. Ding, *Sci. Bull.* **2017**, *62*, 1494.
- [10] J. Yuan, Y. Zhang, L. Zhou, G. Zhang, H.-L. Yip, T.-K. Lau, X. Lu, C. Zhu, H. Peng, P. A. Johnson, M. Leclerc, Y. Cao, J. Ulanski, Y. Li, Y. Zou, *Joule* **2019**, *3*, 1140.
- [11] Y. Jiang, S. Sun, R. Xu, F. Liu, X. Miao, G. Ran, K. Liu, Y. Yi, W. Zhang, X. Zhu, *Nat. Energy* **2024**, *9*, 975.
- [12] L. Zhu, M. Zhang, G. Zhou, Z. Wang, W. Zhong, J. Zhuang, Z. Zhou, X. Gao, L. Kan, B. Hao, F. Han, R. Zeng, X. Xue, S. Xu, H. Jing, B. Xiao, H. Zhu, Y. Zhang, F. Liu, *Joule* **2024**, *8*, 3153.
- [13] L. Zhu, M. Zhang, Z. Zhou, W. Zhong, T. Hao, S. Xu, R. Zeng, J. Zhuang, X. Xue, H. Jing, Y. Zhang, F. Liu, *Nat. Rev. Electr. Eng.* **2024**, *1*, 581.
- [14] C. Li, J. Song, H. Lai, H. Zhang, R. Zhou, J. Xu, H. Huang, L. Liu, J. Gao, Y. Li, M. H. Jee, Z. Zheng, S. Liu, J. Yan, X.-K. Chen, Z. Tang, C. Zhang, H. Y. Woo, F. He, F. Gao, H. Yan, Y. Sun, *Nat. Mater.* **2025**, *24*, 433.
- [15] K. Mullen, W. Pisula, *J. Am. Chem. Soc.* **2015**, *137*, 9503.
- [16] Z. Zheng, H. Yao, L. Ye, Y. Xu, S. Zhang, J. Hou, M. Today, *2020*, *35*, 115.
- [17] Y. Liu, B. Liu, C. Ma, F. Huang, G. Feng, H. Chen, J. Hou, L. Yan, Q. Wei, Q. Luo, Q. Bao, W. Ma, W. Liu, W. Li, X. Wan, X. Hu, Y. Han, Y. Li, Y. Zhou, Y. Zou, Y. Chen, Y. Li, Y. Chen, Z. Tang, Z. Hu, Z. Zhang, Z. Bo, *Sci. China Chem.* **2022**, *65*, 224.
- [18] J. Cao, L. Yi, L. Zhang, Y. Zou, L. Ding, *J. Mater. Chem. A* **2023**, *11*, 17.
- [19] M. Zhang, X. Guo, W. Ma, H. Ade, J. Hou, *Adv. Mater.* **2015**, *27*, 4655.
- [20] Q. Liu, Y. Jiang, K. Jin, J. Qin, J. Xu, W. Li, J. Xiong, J. Liu, Z. Xiao, K. Sun, S. Yang, X. Zhang, L. Ding, *Sci. Bull.* **2020**, *65*, 272.
- [21] C. Sun, F. Pan, H. Bin, J. Zhang, L. Xue, B. Qiu, Z. Wei, Z.-G. Zhang, Y. Li, *Nat. Commun.* **2018**, *9*, 743.
- [22] B. Pang, C. Liao, X. Xu, L. Yu, R. Li, Q. Peng, *Adv. Mater.* **2023**, *23*, 2300631.
- [23] Y. Yang, Z.-G. Zhang, H. Bin, S. Chen, L. Gao, L. Xue, C. Yang, Y. Li, *J. Am. Chem. Soc.* **2016**, *138*, 15011.
- [24] S. M. Swick, W. Zhu, M. Matta, T. J. Aldrich, A. Harbuzaru, J. T. Lopez Navarrete, R. P. Ortiz, K. L. Kohlstedt, G. C. Schatz, A. Facchetti, F. S. Melkonyan, T. J. Marks, *Sci* **2018**, *115*, E8341.
- [25] Z. Luo, T. Liu, H. Yan, Y. Zou, C. Yang, *Adv. Funct. Mater.* **2020**, *30*, 2004477.
- [26] F.-Y. Li, Y.-J. Bai, *J. Energy Storage* **2024**, *94*, 112453.
- [27] J. Wang, P. Wang, T. Chen, W. Zhao, J. Wang, B. Lan, W. Feng, H. Liu, Y. Liu, X. Wan, G. Long, B. Kan, Y. Chen, *Angew. Chem., Int. Ed.* **2025**, *64*, 202423562.
- [28] J. Wang, J. Zhang, Y. Xiao, T. Xiao, R. Zhu, C. Yan, Y. Fu, G. Lu, X. Lu, S. R. Marder, X. Zhan, *J. Am. Chem. Soc.* **2018**, *140*, 9140.
- [29] P. Chao, H. Chen, Y. Zhu, H. Lai, D. Mo, N. Zheng, X. Chang, H. Meng, F. He, *Adv. Mater.* **2020**, *32*, 1907059.
- [30] T. Lin, Y. Hai, Y. Luo, L. Feng, T. Jia, J. Wu, R. Ma, T. A. Dela Peña, Y. Li, Z. Xing, M. Li, M. Wang, B. Xiao, K. S. Wong, S. Liu, G. Li, *Adv. Mater.* **2024**, *36*, 2312311.
- [31] T. Jia, Y. Luo, Y. Hai, T. Lin, X. Qin, R. Ma, K. Fan, A. A. Sergeev, T. A. Dela Peña, Y. Li, M. Li, K. S. Wong, G. Li, J. Wu, S. Liu, F. Huang, *Energy Environ. Sci.* **2024**, *17*, 8593.
- [32] J. V. Grazulevicius, P. Strohriegel, J. Pielichowski, K. Pielichowski, *Prog. Polym. Sci.* **2003**, *28*, 1297.
- [33] S. Wakim, B. R. Aich, Y. Tao, M. Leclerc, *Polym. Rev.* **2008**, *48*, 432.
- [34] J. J. Intemann, E. S. Hellerich, M. D. Ewan, B. C. Tlach, E. D. Spezten, R. Shinar, J. Shinar, M. Jeffries-El, *J. Mater. Chem. C* **2017**, *5*, 12839.
- [35] S. Wen, Y. Li, T. Rath, Y. Li, Y. Wu, X. Bao, L. Han, H. Ehmann, G. Trimmel, Y. Zhang, R. Yang, *Chem. Mater.* **2019**, *31*, 919.
- [36] J. F. Mike, J. J. Intemann, M. Cai, T. Xiao, R. Shinar, J. Shinar, M. Jeffries-El, *Polym. Chem.* **2011**, *2*, 2299.
- [37] A. Bhuwalka, J. F. Mike, M. He, J. J. Intemann, T. Nelson, M. D. Ewan, R. A. Roggers, Z. Lin, M. Jeffries-El, *Macromolecules* **2011**, *44*, 9611.
- [38] H. Sheng, S. Liu, X. Kang, J. Niu, A. A. Adewale, S. Wen, C. Yang, X. Bao, M. Sun, *Nano Energy* **2024**, *126*, 109648.
- [39] D. Qian, L. Ye, M. Zhang, Y. Liang, L. Li, Y. Huang, X. Guo, S. Zhang, Z. a. Tan, J. Hou, *Macromolecules* **2012**, *45*, 9611.
- [40] H. Yao, D. Qian, H. Zhang, Y. Qin, B. Xu, Y. Cui, R. Yu, F. Gao, J. Hou, *Chin. J. Chem.* **36**, 491.
- [41] J. Wang, Y. Cui, Z. Chen, J. Zhang, Y. Xiao, T. Zhang, W. Wang, Y. Xu, N. Yang, H. Yao, X.-T. Hao, Z. Wei, J. Hou, *J. Am. Chem. Soc.* **2023**, *145*, 13686.
- [42] Z. Chen, Y. Xiao, H. Yao, J. Ren, T. Zhang, J. Qiao, S. Zhu, R. Lin, X. Hao, J. Hou, *Adv. Mater.* **2024**, *36*, 2408858.
- [43] G. Wang, J. Wang, Y. Cui, Z. Chen, W. Wang, Y. Yu, T. Zhang, L. Ma, Y. Xiao, J. Qiao, Y. Xu, X.-T. Hao, J. Hou, *Angew. Chem., Int. Ed.* **2024**, *63*, 202401066.
- [44] T. Lu, Q. Chen, *J. Mol. Model.* **2020**, *26*, 315.
- [45] T. Lu, Q. Chen, *J. Comput. Chem.* **2022**, *43*, 539.
- [46] T. Wang, J.-L. Brédas, *J. Am. Chem. Soc.* **2021**, *143*, 1822.
- [47] D. Qian, Z. Zheng, H. Yao, W. Tress, T. R. Hopper, S. Chen, S. Li, J. Liu, S. Chen, J. Zhang, X.-K. Liu, B. Gao, L. Ouyang, Y. Jin, G. Pozina, I. A. Buyanova, W. M. Chen, O. Inganäs, V. Coropceanu, J.-L. Bredas, H. Yan, J. Hou, F. Zhang, A. A. Bakulin, F. Gao, *Nat. Mater.* **2018**, *17*, 703.
- [48] G. Han, Y. Yi, *Acc. Chem. Res.* **2022**, *55*, 869.
- [49] T. Jia, J. Zhang, K. Zhang, H. Tang, S. Dong, C.-H. Tan, X. Wang, F. Huang, *J. Mater. Chem. A* **2021**, *9*, 8975.
- [50] A. Bhuwalka, M. D. Ewan, J. F. Mike, M. Elshobaki, B. Kobilka, S. Chaudhary, M. Jeffries-EL, *J. Polym. Sci., Part A: Polym. Chem.* **2015**, *53*, 1533.
- [51] A. Bhuwalka, M. D. Ewan, M. Elshobaki, J. F. Mike, B. Tlach, S. Chaudhary, M. Jeffries-EL, *J. Polym. Sci., Part A: Polym. Chem.* **2016**, *54*, 316.
- [52] Q. Zhang, B. Kan, F. Liu, G. Long, X. Wan, X. Chen, Y. Zuo, W. Ni, H. Zhang, M. Li, Z. Hu, F. Huang, Y. Cao, Z. Liang, M. Zhang, T. P. Russell, Y. Chen, *Nat. Photonics* **2015**, *9*, 35.
- [53] A. K. K. Kyaw, D. H. Wang, V. Gupta, W. L. Leong, L. Ke, G. C. Bazan, A. J. Heeger, *ACS Nano* **2013**, *7*, 4569.
- [54] P. Schilinsky, C. Waldauf, C. J. Brabec, *Appl. Phys. Lett.* **2002**, *81*, 3885.
- [55] X. Guo, N. Zhou, S. J. Lou, J. Smith, D. B. Tice, J. W. Hennek, R. P. Ortiz, J. T. L. Navarrete, S. Li, J. Strzalka, L. X. Chen, R. P. H. Chang, A. Facchetti, T. J. Marks, *Nat. Photonics* **2013**, *7*, 825.
- [56] G. Wang, S. M. Swick, M. Matta, S. Mukherjee, J. W. Strzalka, J. L. Logsdon, S. Fabiano, W. Huang, T. J. Aldrich, T. Yang, A. Timalsina, N. Powers-Riggs, J. M. Alzola, R. M. Young, D. M. DeLongchamp,

- M. R. Wasielewski, K. L. Kohlstedt, G. C. Schatz, F. S. Melkonyan, A. Facchetti, T. J. Marks, *J. Am. Chem. Soc.* **2019**, *141*, 13410.
- [57] T. A. Dela Peña, R. Ma, Z. Xing, Q. Wei, J. I. Khan, R. M. Young, Y. Hai, S. A. Garcia, X. Zou, Z. Jin, F. L. Ng, K. L. Yeung, D. F. Swearer, M. R. Wasielewski, J. Wang, H. Cha, H. Yan, K. S. Wong, G. Li, M. Li, J. Wu, *Energy Environ. Sci.* **2023**, *16*, 3416.
- [58] Y. Li, R. A. Pacalaj, Y. Luo, K. Ai, Y. Hai, S. Liang, K. Fan, A. A. Sergeev, R. Ma, T. A. Dela Peña, J. S. Müller, Z. Jin, P. S. Tuladhar, T. Jia, J. Wang, G. Li, K. S. Wong, W. Li, J. R. Durrant, J. Wu, *Adv. Mater.* **2024**, 2409212, <https://doi.org/10.1002/adma.202409212>.
- [59] T. Jia, T. Lin, Y. Yang, L. Wu, H. Cai, Z. Zhang, K. Lin, Y. Hai, Y. Luo, R. Ma, Y. Li, T. A. Dela Peña, S. Liu, J. Zhang, C. Liu, J. Chen, J. Wu, S. Liu, F. Huang, *Nat. Commun.* **2025**, *16*, 871.
- [60] C. Lee, S. Lee, G.-U. Kim, W. Lee, B. J. Kim, *Chem. Rev.* **2019**, *119*, 8028.
- [61] T. Jia, J. Zhang, W. Zhong, Y. Liang, K. Zhang, S. Dong, L. Ying, F. Liu, X. Wang, F. Huang, Y. Cao, *Nano Energy* **2020**, *72*, 104718.
- [62] J. Wang, Y. Xie, K. Chen, H. Wu, J. M. Hodgkiss, X. Zhan, *Nat. Rev. Phys.* **2024**, *6*, 365.
- [63] Z. Chen, C. He, P. Ran, X. Chen, Y. Zhang, C. Zhang, R. Lai, Y. Yang, H. Chen, H. Zhu, *Energy Environ. Sci.* **2023**, *16*, 3373.